Available online at www.sciencedirect.com
SCIENCE DIRECT
ELSEVIER
Polymer 46 (2005) 3096–3104
polymer
www.elsevier.com/locate/polymer

Shear-induced crystallization in isotactic polypropylene containing ultra-high molecular weight polyethylene oriented precursor domains

Daniel Dikovsky[a], Gad Marom[a,*], Carlos A. Avila-Orta[b], Rajesh H. Somani[b], Benjamin S. Hsiao[a,**]

[a]*Casali Institute of Applied Chemistry, The Institute of Chemistry, The Hebrew University of Jerusalem, 91904 Jerusalem, Israel*
[b]*Department of Chemistry, State University of New York at Stony Brook, Stony Brook, NY 11794-3400, USA*

Received 24 October 2004; received in revised form 15 December 2004; accepted 20 January 2005
Available online 2 March 2005

Abstract

Melt blends of short ultra-high molecular weight polyethylene (UHMWPE) fibers and isotactic polypropylene (iPP) were subjected to shear at 145 °C, above the melting point of polyethylene (PE). Structural evolution and final morphology were examined by in situ synchrotron X-ray scattering/diffraction as well as ex situ microbeam X-ray diffraction and high resolution scanning electron microscopy, respectively. Results indicate that the presence of oriented UHMWPE molten domains significantly facilitated the crystallization of iPP and enhanced the initial 'shish-kebab' structure leading to the final cylindritic morphology. It is argued that shear flow aligns the fibrillar UHMWPE domains, where the interfacial frictions between PE and iPP effectively retards the relaxation of iPP chains, allowing the aligned iPP chains to create a shish-like structure. Nucleation on the iPP shish initiates the folded chain lamellae (kebabs), which grow perpendicularly to the iPP/PE interface.

Keywords: Shear induced crystallization; UHMWPE fiber; iPP blends

1. Introduction

The interest in understanding the effects of flow on the morphological development in immiscible or partially miscible polymer blends is two faceted, wherein the points of view can focus on either the matrix or the dispersed phase. The main questions that pertain to the first perspective are two: (1) how does the flow induce the matrix crystallization, in particular the nucleation process; and (2) can the dispersed phase interact with the flow and amplify the nucleation effect through interfacial interactions with the matrix. The main question that pertains to the second perspective deals with the orientation capability (a function of viscosity) and the shape factor (e.g. the aspect ratio) of the dispersed phase in the matrix by flow.

It is well known that crystallization of polymer melt under flow (shear or elongation) is enhanced through the formation of orientated molecular arrays, comprising segments of extended chains that are aligned in the flow direction. These molecular arrays can act as nuclei for folded-chain crystallization with growth perpendicular to the flow direction. As a result, polymer processes under varying flow conditions often produce the 'shish-kebab' morphology [1,2], in which the 'shish' consists of aligned extended chains parallel to the flow direction, and the 'kebabs' are made of transversely grown lamellae.

The phenomenon of flow induced molecular orientation and crystallization has been studied quite extensively. These studies dealt with the effects of processing conditions (e.g. temperature, deformation rate and strain) and polymer properties (e.g. molecular weight and distribution). The main factor that controls the flow induced crystallization in polymers is the relaxation time of the deformed chains, which in turn depends on the flow strength and the chain molecular weight. Longer relaxation times are necessary for the formation of stable and oriented nuclei in the polymer melt, as in the case of deforming high molecular weight

* Corresponding authors. Tel.: +972 2 6585898; fax: +972 2 6586068.
** Tel.: +1 631 632 7793; fax: +1 631 632 6518.
E-mail addresses: gadm@vms.huji.ac.il (G. Marom), bhsiao@notes.cc.sunysb.edu (B.S. Hsiao).

0032-3861/$ - see front matter © 2005 Elsevier Ltd. All rights reserved.
doi:10.1016/j.polymer.2005.01.086

polymers at high deformation rates. For a given molecular weight distribution, only a fraction of the polymer chains—above a critical molecular weight [1,3,4]—will remain orientated after deformation, whereby some orientated chain segments will undergo nucleation. It is clear that long chains play an important role in the formation of transient mesophase, which may be an essential step in the flow-induced crystallization.

Recently, several studies have been carried out to understand the effect of high molecular weight fractions on flow induced crystallization in polymer melts using synchrotron X-ray techniques. In relevance to the system investigated in this work, Hsiao and co-workers have carried out studies of shear-induced crystallization in a variety of iPP melts including Ziegler–Natta iPP [5,6], blends of Ziegler–Natta iPP with low and high molecular weight components [3,7,8], diene modified long chain branched iPP [9] and metallocene iPP in blends with atactic polypropylene (aPP) [4]. Their results showed that, after an intense shear flow, orientated primary nuclei ('shish') form first, probably consisting of mesomorphic long chain bundles, which initiate the kebab growth. These observations inspired us to test the idea of enhancing orientation-induced crystallization of a given polymer matrix with a minor polymer component of pre-existing orientation, namely, the blends of iPP matrix and ultra-high molecular weight polyethylene (UHMWPE) short fibers.

A recent study by us showed that UHMWPE domains, immiscible in the iPP matrix, can retain its molecular orientation and effectively induce the iPP 'kebab' nucleation and growth under flow [10]. Wang et al. have also investigated the shear induced 'shish-kebab' structure in iPP and its 50/50 blends with LLDPE, where a model was proposed to explain the morphology in the different phases [11]. In the present study, because the addition of UHMWPE fiber to iPP forms an immiscible blend, the issue of the starting morphology of the dispersed phase (i.e. UHMWPE) must be considered first. This blend system is quite different than conventional immiscible blends under flow, where the spatial arrangement of the dispersed component is mainly developed during the flow and is a function of composition, temperature, viscosity, elasticity ratios of the constituting components and flow strength [12,13]. The geometrical shape of the dispersed phase in conventional immiscible binary blends is generally determined by two parameters, namely the viscosity ratio of the constituting components and the Weber number that depends on the shear rate, the viscosity of the matrix, the size (radius) of the dispersed phase and the interfacial tension of the components [14]. The elongated (fiber-like) geometry of the dispersed domains is of interest in view of its potential reinforcing effect [15]. Accordingly, extensive work has been reported in the literature on in situ formation of microfibrillar structures in different blend systems, such as PP/PA6 [16], EVA/PA6 [17], PP/PET [18], PE/PET [19], and others. Of particular relevance to this study was the investigation dealing with the effects of simultaneous interactions of geometry and crystallization on the morphological formation, such as the formation of the 'shish-kebab' morphology together with transcrystallization of the matrix in a microfibrillar PET/PP blend [20]. The presence of transcrystallinity is expected to have a positive effect on the longitudinal properties of the composite material, as measured in nylon 66 composites [21] and as predicted for iPP composites by in situ microbeam wide-angle X-ray diffraction (WAXD) under stress [22].

The current study investigated melt-mixed polymer blends containing short UHMWPE fibers having high molecular orientation and unoriented iPP, in which the geometry of the polyethylene dispersed domains will be retained in the fibrillar form at the micrometer scale. Furthermore, as the chain relaxation time of UHMWPE is extraordinarily long, high molecular orientation in the UHMWPE phase was expected to be retained even after mixing at high temperatures (i.e. 145 °C, above the equilibrium melting point of PE which is about 141 °C [23]). Hence, this study deals with the question as how the high molecular weight polymer in the dispersed phase with preferred orientation can affect the crystalline morphology of the matrix. A separate study, whose detailed results will be reported elsewhere [10], dealt with the solution-mixed blends of UHMWPE powder and iPP, where the dispersed UHMWPE phase (at sub-micrometer scale) has no preferred molecular orientation. Some results of the solution-mixed UHMWPE powder/iPP blends will also be compared to the melt-mixed UHMWPE fiber/iPP blends.

2. Experimental

2.1. Materials

Melt-mixed polymer blends were composed of Ziegler–Natta isotactic polypropylene (iPP, having a weight average molecular weight, M_w, of 135,000 g/mol, Capilene U77, Carmel Olefins, Israel) and 3 mm long chopped UHMWPE fibers (designated PE_f, Dyneema SK6, DSM, The Netherlands). Solution-mixed blends were prepared from iPP (M_w of 127,000 g/mol and a polydispersity around 3,5, Basell USA,) and UHMWPE powder (designated PE_P, M_w of 6,000,000 g/mol and polydispersity around 9, Basell USA).

2.2. Sample preparations

Melt-blending of iPP with 10% (w/w) chopped fibers, or of as-polymerized powders of UHMWPE, was carried out in a twin-screw microcompounder (DACA Instruments). Blending was performed at 200 °C in two consecutive 10 min cycles. 5% (w/w) antioxidant (Ciba Irganox 3114) was added to prevent polymer degradation at high temperatures. The resulting blends were pressed in a mold to produce 0.5–1 mm thick films, from which ring

specimens of internal diameter and width of 10 and 5 mm, respectively, were cut out by stamping. Solution-mixed blends were carried out by dissolving the composition in xylene and casting films according to the procedure described in [24]. In brief, the mixture was heated slowly to 120 °C with continuous stirring until the polymer was totally dispersed into the xylene (the solution became transparent). The solution was kept at this temperature for 1 h and then poured into iced Methanol. The precipitate was then filtered, washed and dried under vacuum at 70 °C for 48 h.

2.3. Shearing conditions

Shearing stage (Linkam CSS-450) was used to deform the blend. The stage consisted of two parallel circular plates—one stationary and the other rotated by a stepping motor—and diamond and Kapton X-ray windows, to allow in situ X-ray scattering/diffraction measurements. The temperature profile can be precisely controlled by heating and cooling modules to an accuracy of ± 0.2 °C. The ring-shaped sample was sandwiched between two parallel plates on the stage, heated quickly to 200 °C and held at this temperature for 5 min, followed by rapid cooling to 145 °C, where shearing was imposed at a rate of 60 s^{-1} for 5 s. The melt was then allowed to isothermally crystallize for 1.0 h, and then cooled to room temperature at a rate of 30 °C/min. The chosen experimental temperature (145 °C) was above the equilibrium melting temperature of PE, thus the presence of UHMWPE was in the oriented amorphous form.

2.4. WAXD and SAXS measurements

Ex situ microbeam wide angle X-ray diffraction (WAXD) experiments were performed at the European Synchrotron Radiation Facility (ESRF, Grenoble, France) on Beamline ID11. The chosen X-ray wavelength λ was 0.51 Å (the corresponding X-ray energy $E=3$ GV) and the beam diameter was approximately 1.5 μm. The microbeam WAXD patterns were recorded by a Bruker Smart CCD camera (1024×1024, 16 bit, 0.15 mm pixel size). The sample-to-detector distance was 39 cm. The exposure time for each image was 5–30 s. The sample was mounted on a translational stage, equipped with two stepping motors, to allow remote positioning and controlled movement. The X-ray beam was directed perpendicularly to the plan of the ring specimen and the scanning was performed across its width (at right angle to the shear direction).

In situ small-angle X-ray scattering (SAXS) and WAXD measurements were performed at Beamlines X3A2 and X27C, respectively, in the National Synchrotron Light Source (NSLS), Brookhaven National Laboratory (BNL), Upton, NY, USA. The details of the experimental conditions and set-up have been given in [24]. For WAXD measurements, the sample to detector distance was 125.5 mm, calibrated by aluminum oxide (Al_2O_3) as a standard with a wavelength of 1.54 Å. For SAXS measurements, the sample to detector distance was 1688.2 mm, calibrated by silver behenate as standard with a wavelength of 1.36 Å. In both WAXD and SAXS measurements, a CCD camera from MAR-USA with a pixel size of 158 μm was used to collect the scattering data. 2D images were corrected for air scattering and beam fluctuations.

2.5. WAXD data analysis

The WAXD patterns were analyzed using the Polar software (Stonybrook Technology and Applied Research Inc., NY, USA). The radially averaged and azimuthal intensity profiles of the principle diffraction peaks were extracted for every WAXD image. The Origin software was used to plot the radial intensity of the patterns against the Bragg angle, 2θ, which was calculated using $2\theta=\tan^{-1}(R/D)$ with R being the diffraction ring radius and D being the sample to detector distance. The distance between the crystal planes (d) was calculated from the Bragg equation, $n\lambda=2d\sin\theta$. Three dimensional plots (of intensity vs. d vs. position) were generated to show the change in the intensity of the different diffraction peaks with respect to the sample location (the X-ray beam movement).

2.6. Scanning electron microscopy (SEM)

The sheared samples were etched following Bassett's procedure to highlight the crystalline structure [25]. The specimens were coated with Au-Pd nanolayer by SC7640 Sputter. Electron microscopy experiments were carried out with a high resolution scanning electron microscope (HRSEM, FEI Sirion), operated at 10 kV.

3. Results

In situ WAXD/SAXS measurements of UHMWPE/iPP blends were performed using the same procedure employed previously to study flow induced crystallization in UHMWPE/PE blends [24]. Fig. 1 presents a comparison of WAXD images taken at different times after shear during crystallization at 145 °C for three different samples: iPP, iPP/PE_p (10% (w/w)) and iPP/PE_f (10% (w/w)). These diffraction patterns only exhibited the formation of α crystal phase from iPP [7], without any diffraction peak from PE. This confirmed that the presence of UHMWPE was in the amorphous form at the chosen experimental temperature (145 °C). It was seen that the iPP/PE_f blend exhibited the shortest induction time, producing an oriented crystalline diffraction pattern at about 3 min after shear (as seen in the 5 min image of Fig. 1). The crystal orientation indicated that the chains were aligned with respect to the flow direction, which was also consistent with the SAXS results in Fig. 2. Fig. 2(a) shows selected SAXS patterns of the iPP/PE_f blends as a function of time after shear, which reveals that

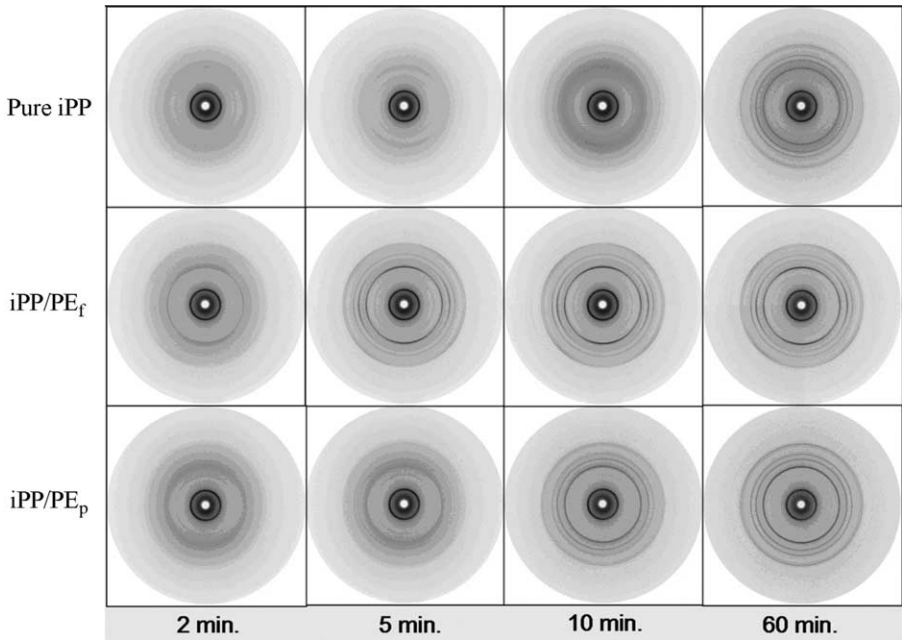

Fig. 1. Selected in situ WAXD images of sheared iPP homopolymer and polymer blends at varying crystallization times at 145 °C.

the orientated lamellar structure is aligned perpendicularly to the flow direction, where the iPP chains are parallel to the flow direction. Fig. 2(b) shows the SAXS patterns collected at 60 min after shear for the iPP/PE_f blends of three different compositions (0, 5 and 10% (w/w)). It is interesting to note that the formation of orientated lamellar structure in the

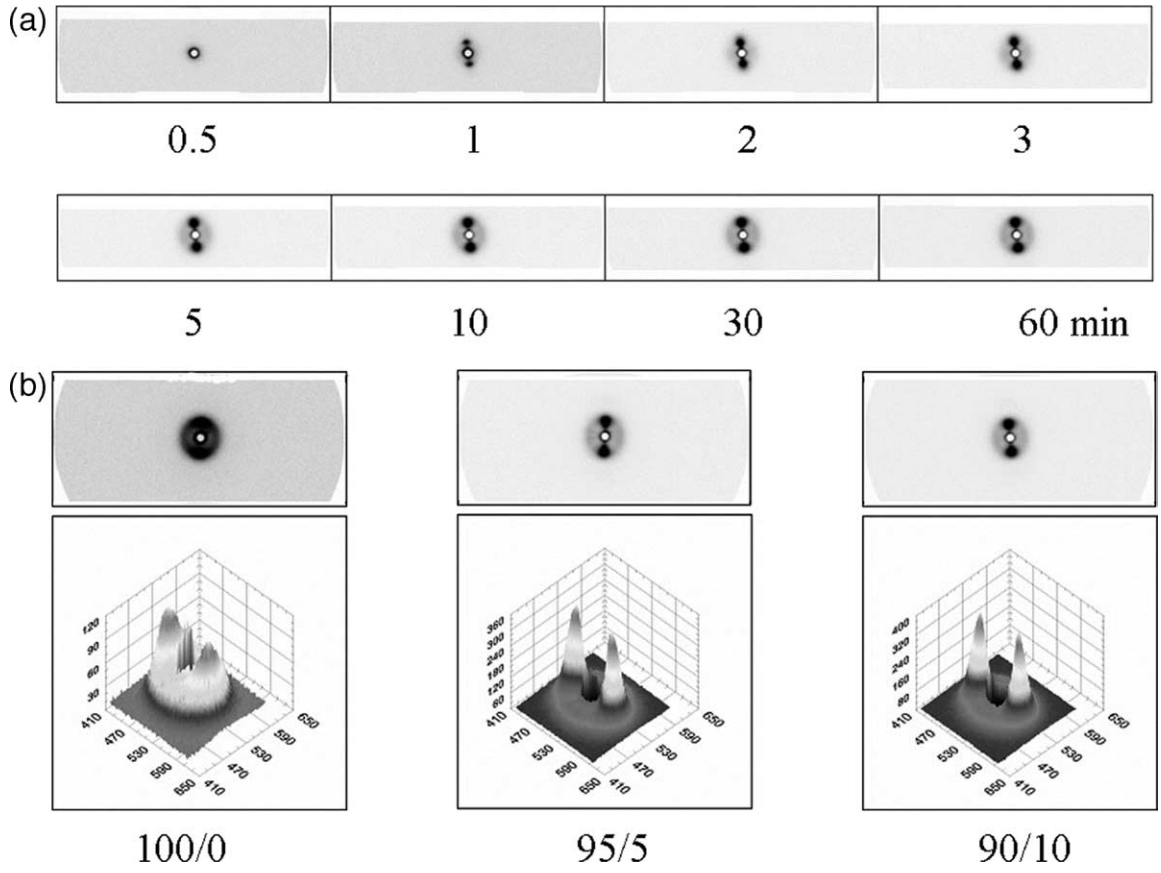

Fig. 2. Selected in situ SAXS results of sheared iPP compositions: (a) of the iPP/PE_f (10% (w/w)) blend as a function of time; and (b) of three compositions of the iPP/PE_f blends at 60 min after shear.

blend of 5% (w/w) PE_f is significantly more pronounced than that of the pure iPP, but is similar to that of the blend with 10% (w/w) PE_f. This crystal orientation was found to be very uniform across the width of the specimen, and was aligned perpendicularly to the shearing direction. An example microbeam WAXD profiling of fully crystallized sheared iPP sample in an interval step of 2 μm is shown in Fig. 3, where the azimuthal histograms of (110) and (040) reflections show the appearance of constant profiles regardless of the relative position across the width of the specimen.

It is emphasized that a complete set of control experiments, including the pure iPP and the blends, had been performed in the absence of shear (namely, under quiescent conditions) at the same isothermal conditions (145 °C). However, both the in situ WAXD and SAXS results showed no signs at all of any crystallization or morphology formation in the absence of shear even after 60 min. Only thereafter, upon cooling to ambient temperature, did the materials crystallize. These observations confirmed that shear application was essential for inception of crystallization, as already reported [3–8].

The presence of PE domains was determined by the appearance of the (200) and (110) diffraction peaks ($d=3.7$, 4.2 Å, respectively) from PE crystals in the microbeam WAXD profile, as shown in Fig. 4. Fig. 5 shows a series of diffraction profiles taken at different positions across a single orientated PE_f domain in the fully crystallized sheared iPP sample at room temperature (the observed PE domain width was around 50 μm, where the original fiber width was around 25 μm). In addition, the PE domain was immersed in the iPP matrix, where both iPP and PE crystal reflections were detected simultaneously. These profiles were further analyzed to characterize the effect of iPP and PE interactions on the crystal orientation of the iPP matrix. Fig. 6 shows the width at half-height of azimuthal intensity profiles taken at the (110) and (040) reflections for iPP crystals as a function of the distance from the iPP/PE_f interface, where the interface is marked with the dotted line

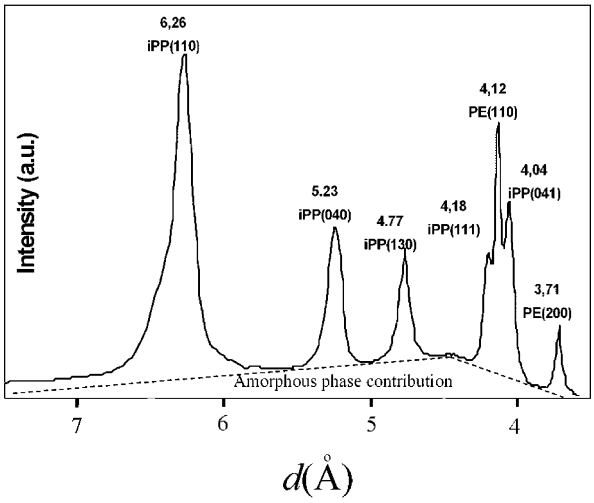

Fig. 4. Typical microbeam WAXD profile of an iPP/PE_f specimen penetrated through one PE domain showing the superposition of multiple iPP reflections and two PE reflections ((200) and (110)).

(the left side represents the pure iPP matrix and the right side represents the iPP/PE superimposed domain). It is interesting to note that a sharp increase in the value of the width at half-height is seen near the interface, indicating a sharp decrease in the degree of iPP crystal orientation in the vicinity of the interface.

SEM examinations of the etched surfaces from cross-sectioned samples provide important morphological information on the lamellar orientation of both iPP and PE phases in the blend. Fig. 7 shows a typical SEM image of lightly etched surface of the cross-sectioned sample, showing a PE_f inclusion having an irregular shape in the iPP matrix (the general flow direction is marked with the arrow). In the iPP matrix, several 'shish' and 'kebab' structures can be identified parallel and perpendicular to the flow direction, respectively, even at this relatively low magnification. In the PE_f domain, the PE lamellae at the interface between iPP and PE seem to form highly ordered stacks, oriented perpendicularly to the interface. This feature becomes more enhanced at a higher magnification

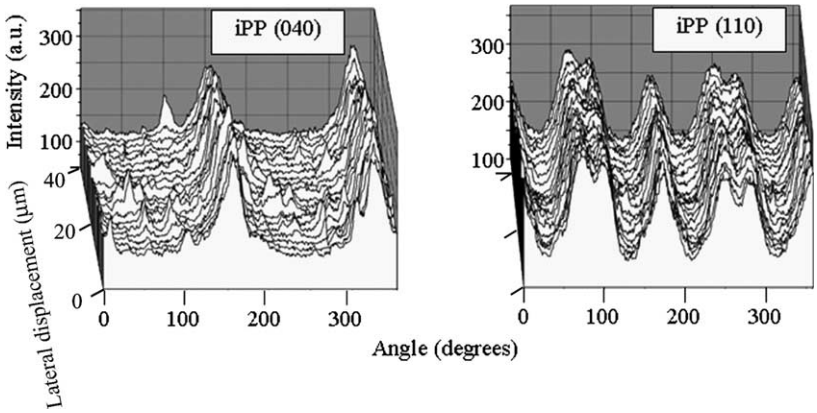

Fig. 3. Azimuthal profiles of the (110) and (040) reflections for pure iPP as a function of the distance across the width of the sheared specimen (the data extracted from the microbeam WAXD, where the X-ray beam movement was perpendicular to the flow direction).

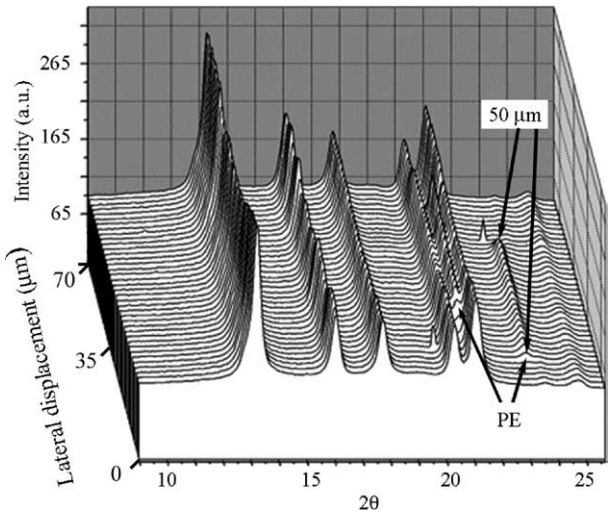

Fig. 5. A series of diffraction profiles at 2 μm intervals across the width of one PE_f domain in the iPP/PE_f specimen, showing both PE (200) and (110) reflections (the domain width was about 50 μm).

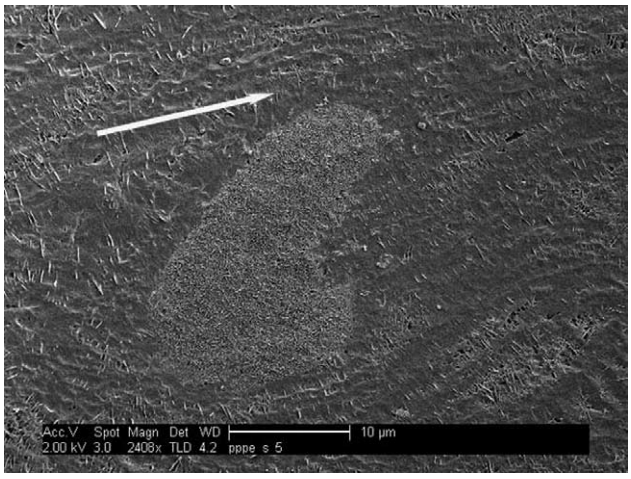

Fig. 7. High resolution SEM image of the surface-etched cross-sectioned iPP/PE_f specimen, where the PE domain is near the center (the arrow marks the flow direction).

of the SEM image in the PE domain (Fig. 8(a)). The typical shish-kebab structure in the iPP matrix is shown in Fig. 8(b). Fig. 9 shows the typical cross-sectioned SEM images of liquid nitrogen freeze-fractured and chemically etched iPP domains, where the flow direction is perpendicular to the observation plan. A host of closely packed iPP cylindrites is seen in Fig. 9(a), which is consistent with the formation of the 'shish-kebab' precursor structure induced at the initial stage of crystallization. In some cases, the etching procedure removed some material between cylindrites, enabling a closer examination along the stem of the cylindritic structure. This is shown in Fig. 9(b) and (c), revealing stacks of circular lamellae, whose the a^*–b^* plans are perpendicular to the stem axis and are consistent with the 'shish-kebab' model [1].

In the solution-mixed iPP/PE_p blends, despite the notion that the PE domains were in the amorphous state during deformation at high temperatures [10], the SEM image of the

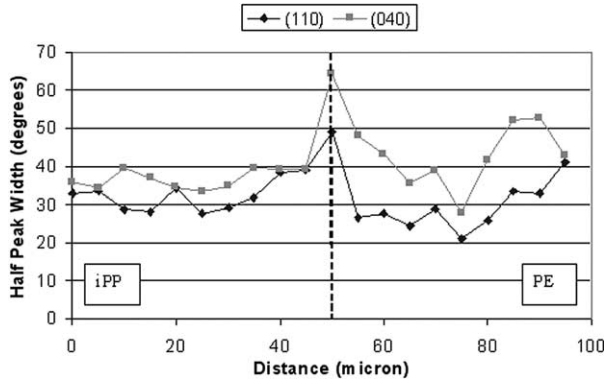

Fig. 6. The width at half-height of azimuthal profiles take at the (110) and (040) reflections of iPP crystal as a function of the distance from the iPP/PE_f interface (the interface is marked with the dotted line, the left side represents pure iPP domain, the right side represents the iPP/PE_f superimposed region).

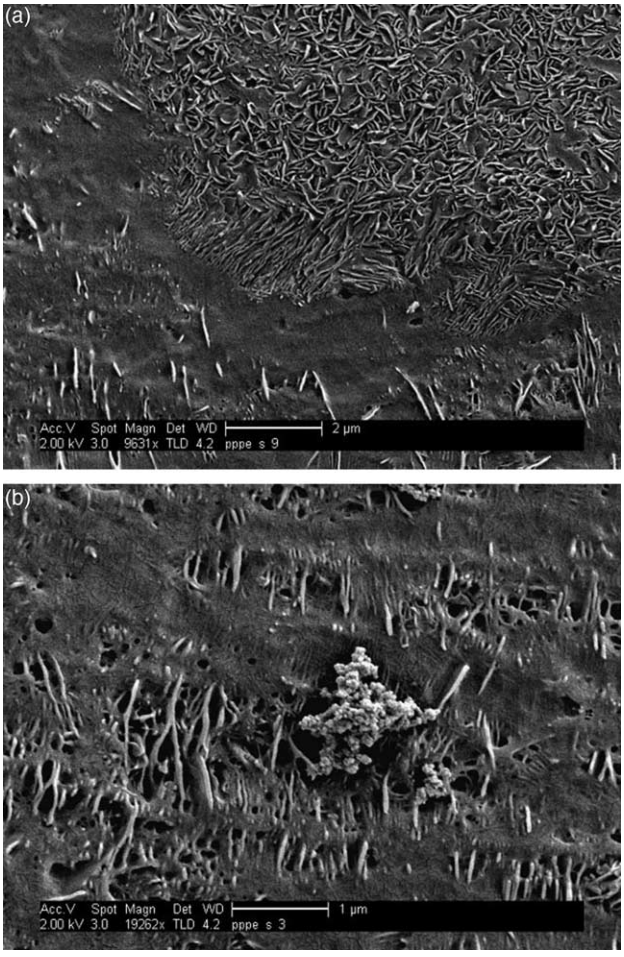

Fig. 8. Higher magnification SEM images of Fig. 7, showing (a) the iPP/PE_f interface, where the ordered PE lamellar stacks are orientated perpendicularly to the interface (the shear flow direction is roughly from left to right); (b) the 'shish-kebab' morphology in the iPP matrix.

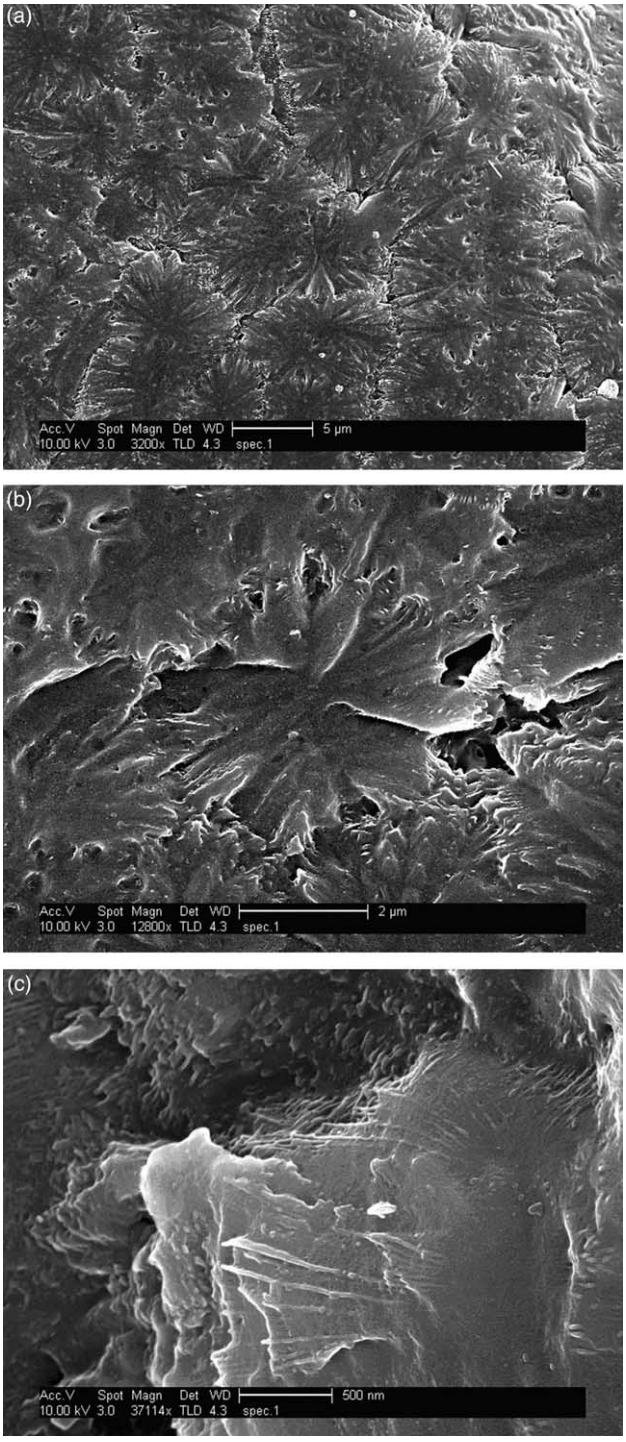

Fig. 9. SEM images of liquid nitrogen freeze-fractured and chemically etched cross-sections of the iPP domain, showing: (a) closely packed cylindrites; (b) a view along the 'shish' axis of a cylindrite, revealing kebab-like lamellar stacks; (c) a higher magnified view of a lamellar stack. (The flow direction is perpendicular to the observation plan).

etched surface of the sheared sample reveals small crystalline domains of PE (Fig. 10). It is seen that the PE_p domains were about two orders of magnitude smaller than those of the PE_f domains. However, unlike the PE_f domains, the PE_p domains do not exhibit an ordered lamellar morphology at the interface.

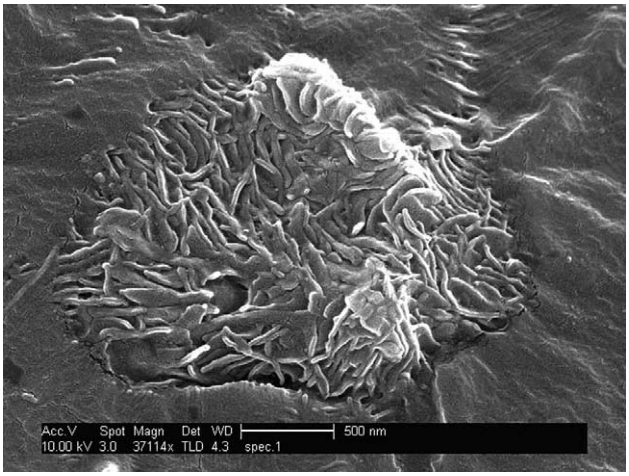

Fig. 10. High resolution SEM of the etched iPP/PE_p solution-mixed sample, focusing on the crystalline PE domain.

Finally, it is noted that, by and large, the PE_f segments did not acquire a marked elongated shape with the shear flow, where different shapes and geometries of the UHMWPE domains could be seen in Fig. 7. A low magnification SEM of etched cross-section is presented in Fig. 11 to show the cylindritic morphology in the iPP matrix close to a PE segment that protrudes from the cross-section.

4. Discussion

The microbeam WAXD profiles showed a high level of anisotropy in the iPP domains relative to the shear direction (Fig. 3). The appearance of equatorial reflections of the (040) plan (parallel to the b^*-axis) and the (110) plan (the vector sum of both a^* and b^*-axes) indicates that the a^*–b^* plan lays perpendicularly to the shear direction. In addition, four (110) reflections, inclined at $\pm 75°$ to the equator of the

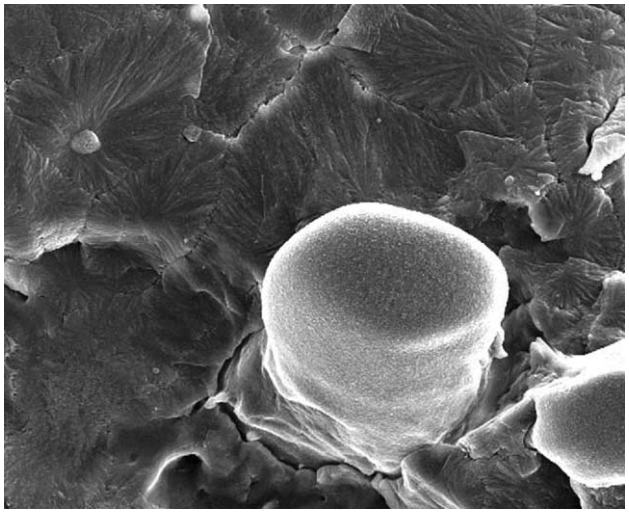

Fig. 11. Etched iPP/PE_f surface with an elongated protruding PE segment surrounded by iPP cylindrites.

parent lamellae, can be attributed to the daughter lamellae, which has been discussed elsewhere [26]. This conclusion and the above morphological observations of orientated cylindritic structures suggest the following pathway for the structural formation of this blend under shear, which is shown in Fig. 12.

Based on results in Figs. 1 and 2, it is apparent that the presence of immiscible oriented UHMWPE domains facilitates the crystallization kinetics of the surrounding iPP matrix. The possible mechanism for this behavior is as follows. During shear, the principal axis of UHMWPE fibers tends to align with the flow direction. As the chain relaxation time of UHMWPE is extraordinarily long, it allows the retention of molecular orientation, at a significant degree, in the molten PE domain. However, the PE chains at the interface probably become more mobile than the core chains because the surrounding iPP chains have much lower relaxation times. The viscosity levels for both PE and iPP chains are thus modified based on the double reptation mixing rule [27] due to some degree of mutual diffusion. This would lead to two effects: (1) the interfacial PE chains would decrease their relaxation times, and thus lose the molecular orientation that is consistent with the SEM observations (Fig. 8) and the microbeam WAXD results (Fig. 6); and (2) the interfacial iPP chains will increase their effective relaxation times, which leads to the retention of its molecular orientation after flow and creates the shish-like structure that promotes the kebab (lamellar) growth perpendicularly to the fiber axis (Fig. 12, right diagram). Nucleation of iPP is thus enhanced at the surface of the PE domain. The shish-kebab formation at the initial stage of flow-induced crystallization forms the basis for the cylindrites morphology.

5. Conclusions

The presence of micrometer size domains of oriented but non-crystalline UHMWPE domains in iPP significantly enhances shear-induced crystallization and orientation of the iPP matrix. At 145 °C, the timescale for the appearance of orientated iPP morphology was approximately 2 min. High resolution SEM of freeze-fractured and etched surfaces showed that the resulting morphology comprised a closely packed iPP cylindrites, aligned in the shear flow direction. The PE domains acquired only a marginal elongated shape due to the shear flow conditions upon melting. We argue that the hydrodynamic interactions between the long PE chains and relatively short iPP chains significantly retards the relaxation times of surrounding iPP chains, resulting the formation of oriented nuclei (shih-like) at the interface. These oriented iPP nuclei would enhance the development of kebab and result in the cylindrites morphology.

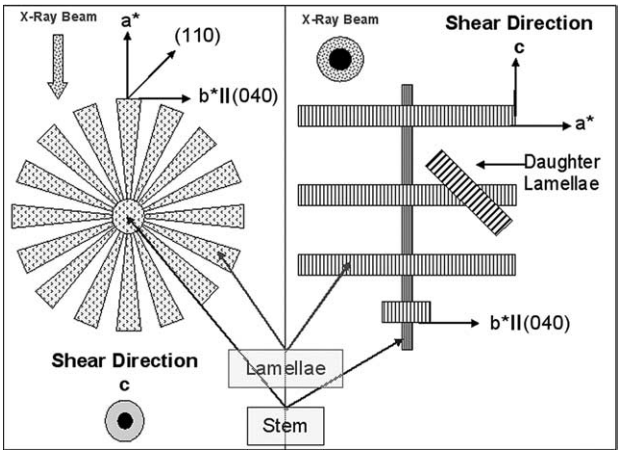

Fig. 12. A model of the cylindritic morphology of the iPP matrix in the blend with respect to the shear flow direction, illustrating *a**, *b** and *c*-axes of the parent lamellae.

Acknowledgements

The research of the Israeli authors was supported by the Israel Science Foundation (grant no. 40/01). The US team thanks the financial support of the National Science Foundation (DMR-0405432).

References

[1] Keller A, Kolnaar HWH. Mater Sci Technol 1997;18:189.
[2] Eder G, Janeschitz-Kriegl H. Mater Sci Technol 1997;18:268.
[3] Somani RH, Hsiao BS, Nogales A, Srinivas S, Tsou AH, Sics I, et al. Macromolecules 2000;33:9385.
[4] Somani RH, Yang L, Hsiao BS, Fruitwala HJ. Macromol Sci Phys 2003;B42:515.
[5] Somani RH, Yang L, Hsiao BS, Agarwal PK, Fruitwala H, Tsou A. Macromolecules 2002;35:9096.
[6] Somani RH, Yang L, Hsiao BS. Physica 2002;A304:145.
[7] Somani RH, Hsiao BS, Nogales A, Fruitwala H, Srinivas S, Tsou A. Macromolecules 2001;34:5902.
[8] Nogales A, Hsiao BS, Somani RH, Srinivas S, Tsou AH, Balta-Calleja FJ, et al. Polymer 2001;42:5247.
[9] Agarwal PK, Somani RH, Weng W, Mehta A, Yang L, Ran S, et al. Macromolecules 2003;36:5226.
[10] Avila-Orta CA, Somani R, Yang L, Burger C, Marom G, Hsiao BS. Polymer. Submitted for publication.
[11] Wang Y, Na B, Fu Q, Men Y. Polymer 2004;45:207.
[12] Han CD. Multiphase flow in polymer processing. New York: Academic Press; 1981.
[13] Utracki LA. Polymer alloys and blends. Munich: Hanser Publishers; 1990.
[14] Taylor GI. Proc R Soc Lond 1934;A146:501.
[15] Fakirov S, Evstatiev M, Friedrich K. Microfibrillar reinforced composites—another approach to polymer blends processing. In: Paul DR, Bucknall CB, editors. Polymer blends. Performance, vol. 2. New York: Wiley; 1999. p. 455.
[16] Li XD, Chen MC, Huang YH, Cong GM. Polym Eng Sci 1999;39:881.
[17] Tzur A, Narkis M, Siegmann A. J Appl Polym Sci 2001;82:661.
[18] Chen M, Huang Y, Zhao S, Cong G. J Appl Chem—USSR 1995;12:77.
[19] Li ZM, Yang MB, Huang R, Yang W, Feng JM. Polym Plast Technol Eng 2002;41:19.

[20] Li ZM, Li LB, Shen KZ, Yang W, Huang R, Yang MB. Macromol Rapid Commun 2004;25:553.
[21] Nuriel H, Klein N, Marom G. Compos Sci Tech 1999;59:1685.
[22] Assouline E, Grigull S, Marom G, Wachtel A, Wagner HD. J Polym Sci, Polym Phys 2001;39:2016.
[23] Yamajaki S, Hikosaka M, Toda A, Wataoka I, Yamada K, Tagashira KJ. Macromol Sci, Part B Phys 2003;B42:499.
[24] Yang L, Somani RH, Sics I, Hsiao BS, Kolb R, Fruitwala H, et al. Macromolecules 2004;37:4845.
[25] Bassett DC, Hodge AM. Proc R Soc Lond 1981;A377:25.
[26] Assouline E, Wachtel A, Grigull S, Lustiger A, Wagner HD, Marom G. Polymer 2001;42:6231.
[27] des Cloizeaux J. J Europhys Lett 1988;5:437.